Helium isotope evidence for cryptic magmatism along Central France

Carolina Dantas Cardoso, Emma Russier, Bernard Marty, Raphaël Pik, David Bekaert, Alan Seltzer, Michael Broadley, David Byrne, Thomas Rigaudier, Yves Géraud, et al.

TITLE

Helium isotope evidence for cryptic magmatism along Central France

AUTHORS

Carolina Dantas Cardoso[a,*], Emma Russier[b,c], Bernard Marty[a], Raphaël Pik[a], David V. Bekaert[a,d], Alan Seltzer[d], Michael W. Broadley[a], David Byrne[a], Thomas Rigaudier[a], Yves Géraud[b], Alexandre Tarantola[b], Benoît Hauville[c]

AFFILIATIONS

[a]Université de Lorraine, CNRS, CRPG, F-54000 Nancy, France

[b]Université de Lorraine, CNRS, GeoRessources, F-54000 Nancy, France

[c]45-8 Energy, Metz 57000, France

[d]Marine Chemistry and Geochemistry Department,Woods Hole Oceanographic Institution, Woods Hole, Massachusetts 02543, USA.

ABSTRACT

Determining the source(s) of helium in regions of the crust where ^{3}He anomalies occur can be challenging when no surface manifestations of magmatic activity or a clear active extension regime are present. This is the case of the Paris basin (France), where geothermal fluids and oils ^{3}He/^{4}He have been previously shown to range from 0.02 R_a up to 0.14 R_a (Marty et al., 1993; Pinti & Marty, 1995, 1998), whereas natural gases to the south of the Paris Basin (near the Massif central) show unambiguous evidence for mantle helium contribution, with ^{3}He/^{4}He up to 6.4 R_a (Bräuer et al., 2017). However, higher ^{3}He/^{4}He than the crustal endmember (~ 0.01 R_a), as observed in the Paris Basin, could be a sign of either (i) a weak contribution of mantle He (enriched in primordial ^{3}He) or (ii) the contribution of ^{3}He naturally produced by nuclear reactions of lithium, for which commercially exploitable concentrations have been reported in rare-metal-rich granites. One way to distinguish between these two possibilities is to combine He isotope systematics with other noble gas tracers of mantle inputs, such as xenon isotopes. Here, we report the isotope compositions of helium and xenon, measured by static and dynamic mass spectrometry, respectively, in gas samples collected in the Nièvre County, between the Massif Central and the Paris Basin. ^{3}He/^{4}He ratios range between 0.16 and 0.22 Ra. Combined with previous studies, our data are consistent with

a southward increase of He isotope ratios along major fault systems from the Paris Basin (~ 0.02 R_a) towards the Massif Central (6.4 R_a). This geographical trend, paired with high precision Xe isotopes exhibiting an excess of mantle ^{129}Xe, shows a clear mantle input that is most likely restricted to the major fault systems in Central France. The occurrence of mantle-derived helium and xenon in Central France highlights the presence of cryptic magmatism in areas with no apparent volcanic manifestations.

Keywords: noble gases; helium isotopes; xenon isotopes; mantle input; CO_2 reservoir

1 Introduction

On Earth, the two helium isotopes, ^3He and ^4He, are found in the atmosphere, crust, and mantle in different proportions. ^3He is mainly of primordial origin, occurring in higher proportions in the mantle, where it has been able to be preserved since Earth's accretion (Craig & Lupton, 1976). ^4He on the other hand is primarily of radiogenic origin and is concentrated in the continental crust (Ballentine & Burnard, 2002). The production of ^4He primarily occurs by α-decay of $^{235,238}U$ and ^{232}Th, and is thus dependent on the concentration of these two parent elements (Ballentine & Burnard, 2002). However, production of ^3He can also occur in the crust produced through the thermal neutron capture on ^6Li by the reaction ^6Li (n,α) ^3H (β^-) → ^3He (Morrison & Pine, 1955).

The $^3He/^4He$ ratio is thus an essential tool for determining the origin of different gas reservoirs. In some regions of the crust, the interpretation of $^3He/^4He$ can be ambiguous, such as in the Paris Basin (France), where no magmatic manifestations at the surface, or evidence for modern tectonic extension are present, yet helium isotope ratios show higher $^3He/^4He$ than expected for the continental crust (up to 0.14 Ra; Marty et al., 1993; Pinti & Marty, 1995, 1998). Helium isotopes have been investigated in groundwater and crude oil from the Paris Basin and in gas manifestations in the Massif Central, respectively (Bräuer et al., 2017; Marty et al., 1993; Pinti & Marty, 1995, 1998). While there is unequivocal evidence for a mantle contribution in the Massif Central, with $^3He/^4He$ ratios up to 6.4 R_a (where R_a is the atmospheric $^3He/^4He$ – 1.39 x 10^{-6}; Graham, 2002), a mantle contribution in the Paris Basin is less evident. Helium isotope ratios (0.02 – 0.11 R_a, reaching 0.14 R_a for basement-hosted groundwater) are close to the crustal end-member (0.001 – 0.02 Ra) as computed from average U+Th/Li abundances in related lithologies of the Paris Basin (Pinti & Marty, 1998). Because $^3He/^4He$ ratios of geothermal fluids and oils are higher than values predicted for a purely

crustal origin, Pinti and Marty (1998) proposed a mantle contribution to gases hosted by basinal fluids. In agreement with this possibility, it was observed that the $^{3}He/^{4}He$ ratios increase with depth in the basin, suggesting injection of mantle-derived helium from the basement underlying the sedimentary units, and progressive dilution of this signal by radiogenic, ^{4}He-rich helium produced in the sedimentary pile (Marty et al., 1993). Helium isotope ratios also tend to be higher towards the southern margin of the basin (0.09 Ra in groundwater and 0.14 Ra at the basement; Pinti and Marty, 1998). This trend is possibly related to the North-South major fault system ("Sillon Houiller") in Central France, and to the addition of mantle-derived ^{3}He from the nearby Rhine rift magmatism at the eastern border of the Paris Basin in Lorraine (Marty et al., 2003). Alternatively, $^{3}He/^{4}He$ ratios higher than expected for the purely crustal end-member could reflect local enrichments of lithium-derived ^{3}He, with He isotope variations potentially tracking the occurrence of Li-rich lithologies of economical relevance.

Recently, a CO_2-rich gas reservoir with He concentration reaching 0.04% has been discovered while conducting helium exploration in the Nièvre County, between the Massif Central to the south and the southern border of the Paris Basin to the north (Fig. 1). Although not reaching commercial concentrations for helium (> 0.3%), its helium content is about 100 times higher than the atmosphere (~ 0.0005%; Glueckauf, 1946). This gas accumulation has the potential to shed light into the nature of the intermediate $^{3}He/^{4}He$ ratios, between typical mantle values and the crustal range, observed in the Paris Basin (e.g., Pinti and Marty, 1998). The geochemical description of this reservoir is still at an early stage, and so our paper focuses on the use of isotope geochemistry to identify the source(s) of the Nièvre gas.

In the present study, we sampled bulk gas samples using two distinct approaches: copper tubes (dedicated to He isotope measurements) and Giggenbach bottles (dedicated to Ar-Ne-Xe isotope measurements). The samples consist in free gases from two CO_2-rich wells (SP4 and SP7) and bubbling springs from the surrounding areas – Gelin, Fonts-Bouillants, Fontaine des Vertus, Pougues-les-Eaux, Fontaines Salées, and Bourbon-Lancy (Fig. 1). Most springs were cold (12-14°C; Boineau & Maisonneuve, 1972; Risler, 1974), apart from Bourbon-Lancy, which has a temperature of 52°C (Batard et al., 1982). To identify the different sources of helium, we analysed $^{3}He/^{4}He$ and $^{4}He/^{20}Ne$ on gas collected from all sites. We also analysed the major gas

composition, stable isotopes of CO_2 ($\delta^{13}C$) and N_2 ($\delta^{15}N$), and Ar, Ne, and Xe isotopes for the SP4 and SP7 well gas samples.

2 Geological setting

The study area is located between the southern border of Paris Basin and the north of the Massif Central and Limagne basin, west of the Morvan massif (Fig. 1). The Massif Central and Morvan belong to the Hercynian belt. The basement of the basin is made up of Hercynian granites, migmatites, gneisses and mica schists that outcrop in the Decize horst (Clozier and Turland, 1982; Roger et al., 2010). The study zone is also likely to contain uranium-rich carboniferous and permian deposits, mostly alternating clay and sandstone, that formed during the dismantling of the Variscan belt under the Mesozoic and Cenozoic cover (Beccaletto et al., 2015; Farjanel, 1989; Mercuzot et al., 2021).

The area underwent magmatic and volcanic activity during the Hercynian period and Paleogene (Baptiste, 2016; Farjanel, 1989). The emplacement of the Decize and Montmarault granitic intrusion (321 ± 2 Ma U-Th-Pb dating on monazite; Joly, 2007) and rare metal-enriched granites in the Morvan and Massif Central took place as the belt began dismantling (Gloaguen et al., 2018; Roger et al., 2010). The most recent volcanic activity occurred during the Paleogene, at ~90 km to the South of the Paris Basin, in "Chaîne des Puys" related to the Alpine orogeny and the Cenozoic extension regime (Barruol & Granet, 2002). The origin of volcanism in the area is still debated (Nehlig et al., 2003). On the one hand, it could reflect the surface expression of a mantle plume (Coisy & Nicolas, 1978; Froidevaux et al., 1974), as potentially suggested by seismic tomography (Mazabraud et al., 2005), originating from the asthenosphere related to the activity of a hot spot (Froidevaux et al., 1974) or to a passive rift (Merle & Michon, 2001). On the other hand, volcanism may result from crustal extension and melting of the lithospheric material (Gautheron et al., 2005). One last possibility is that a deep plume led to the formation of shallower plumes in the Sub Continental Lithospheric Mantle (SCLM) and/or in the old oceanic lithosphere crust (~ 400 Ma subduction during the Hercynian orogeny) (Buikin et al., 2005; Gautheron et al., 2005). Noble gas data from the Massif Central, namely Xe and Ne isotopes, indicate a MORB-like source, discarding the influence of a mantle plume (Moreira et al., 2018).

Seismicity is not restricted to the Massif Central and seismic events have been recorded along the major structures of the area (Marche and Sillon Houiller faults).

Most faults appear to be related to the complex geodynamic history of the area (Variscan subduction, collision, and exhumation) and are deeply embedded in the basement, such as the Sillon Houiller and Loire faults (Baptiste, 2016; Regorda et al., 2020; Roger et al., 2010; Vanderhaeghe et al., 2020). The Magnetic Paris Anomaly follows the same N-S orientation as the Loire fault in the North of Massif Central. Even if its origin is debated, this anomaly could be linked to a deep major structure, such as a main strike-slip fault or an oceanic suture covered by the Paris Basin sediments (Baptiste, 2016). Variscan faults oriented N20-30 have been reactivated into shear and then normal faults during the formation of the Carbonifereous pull-out and Permian hemi-graben (Beccaletto et al., 2015; Farjanel, 1989). They were also reactivated by extension and compression at the end of the Jurassic (E-W) during the opening of the Tethys, amid the Cretaceous (SW-NE extension and N-S compression) and the W-E extension in the Tertiary (Guillocheau et al., 2000; Jolivet et al., 2021; Manatschal et al., 2021; Roger et al., 2010). Gas-rich springs and drillings are located along faulted areas with mainly N-S directions. SP4, SP7, Gelin, Fonts-Bouillants, and Fontaine des Vertus follow a single fault, the Saint-Parize-le-Châtel fault while Pougues-les-Eaux is located in an area affected by multiple normal faults. Bourbon-Lancy and Fontaines Salées are situated along Morvan bounding fault.

3 Methods

3.1 Bulk gas compositions

Gases occur either as bubbles in springs (Gelin, Fonts-Bouillants, Fontaine des Vertus, Pougues-les-Eaux, Bourbon-Lancy and Fontaines Salées) or as free CO_2-rich gas in two drill holes (SP4 and SP7). Samples were collected during three field campaigns and/or well testing operations, in August-September, 2021, February and May-June, 2022 (Table 1). SP4 and SP7 drill holes are rooted in the Triassic sediments and cross the Saint-Parize-le-Châtel fault. Gases were sampled in evacuated vials or Tedlar Bags after purging the tubes connecting them to the wellheads. The springs near SP4 (Gelin, Fonts-Bouillants, Pougues-les-Eaux, and Fontaine des Vertus) were sampled before and after the well test to detect potential variations in helium isotopes. Bubbling gases from springs were collected through funnel and Teflon tubing in previously evacuated vials (Pasquet et al., 2021) or Tedlar bags (Battani et al., 2010). Finally, the gas composition was measured by gas chromatography (GC) (Supplementary material; Pasquet et al., 2021).

3.2 Noble gases

3.2.1 $^{3}He/^{4}He$ and $^{4}He/^{20}Ne$

The analyses of $^{4}He/^{20}Ne$ and $^{3}He/^{4}He$ ratios of gases sampled in copper tubes were performed, respectively, on a MKS Microvision 2 quadrupole mass spectrometer (QMS) and a split flight tube noble gas mass spectrometer (Helix SFT - Thermo Fisher Scientific) at the Centre de Recherches Pétrographiques et Géochimiques (CRPG) noble gas analytical facility (Mabry et al., 2013). The standard deviation of the $^{3}He/^{4}He$ ratios ranged from 1.4 to 3.7 % based on the replicate analysis of standard He (atmospheric). Results are corrected for blanks, which contributed < 0.1 % of the total He abundances (Table 2).

3.2.2 Ar, Ne, and Xe isotopes

Gases were collected in 1.5 L Giggenbach bottles (Giggenbach & Goguel, 1988; Bekaert et al. 2019) containing 4N NaOH solution in which CO_2 and other reactive species (e.g., S compounds) can be trapped. This method permits the concentration of inert gases (mainly N_2 and noble gases and possible traces of CH_4, CO, H_2, etc) in the vacuum headspace above the solution. In the laboratory, the gaseous fraction was equilibrated under vacuum with an evacuated metal bottle fitted with two metal valves (Nupro SS4H$^{@}$), where the gas could be stored for long periods of time without diffusive leakage or exchange with atmospheric gases. Aliquots of gas were expanded in a vacuum line and the abundances of He and Ar as well as Ar isotopic ratios were measured after purification via static mass spectrometry on a GV Helix MC mass spectrometer. Two aliquots of the SP4 well gas were also sampled from the metal bottles and analysed for all noble gases (Table 3). Gases were purified using hot (600°C) and cold (25°) Ti-getters and, after cryogenic separation (Broadley et al., 2022), noble gas abundances and isotopic ratios were analysed with a Helix MC+ mass spectrometer at the Centre de Recherches Pétrographiques et Géochimiques (CRPG) noble gas analytical facility (Bekaert et al., 2019; Broadley et al., 2020).

At last, argon and xenon isotope ratios were measured in the Seltzer Lab at Woods Hole Oceanographic Institution via dynamic isotope-ratio mass spectrometry (Bekaert et al., 2023; Seltzer & Bekaert, 2022) for one sample of the SP7 well gas collected in a large Giggenbach bottle (1.5 L) following the sampling procedure detailed by Bekaert et al. (2019). With a dynamic mass spectrometer, often called an “isotope ratio mass spectrometer,” the rapid switching between analysis of sample and reference

gas streams reduces the effect of instrumental drift (McKinney et al., 1950) and allows for many comparable measurements of purified sample gas and standard gas of known isotopic composition over the course of an analysis, hence ensuring accurate and unbiased isotopic ratio determination at the sub-per mil level. Results are in permil (‰) and notated as δ following $\delta R = \left[\left(R_{sample}/R_{atmosphere}\right) - 1\right] \times 1000$; where R is a Xe isotope ratio. Raw measurements were corrected for diffusive transport fractionation (DTF; light isotope enrichment due to physical subsurface fractionation; Bekaert et al., 2023) using $\delta^{128}Xe/^{130}Xe$, yielding a mass-dependent correction of 0.504 ± 0.157 ‰ u^{-1}. Our reported uncertainties on Xe isotope data reflect both analytical and DTF-correction sources of uncertainty (Table 3).

3.3 Stable isotopes

The carbon and nitrogen isotopic compositions of CO_2 and N_2, respectively, were measured with a Thermo Scientific MAT 253 Mass Spectrometer at the Centre de Recherches Pétrographiques et Géochimiques (CRPG) stable isotopes analytical facility. Sampling was performed using Giggenbach bottles and evacuated glass bottles.

3.3.1 $\delta^{13}C$

For the $\delta^{13}C$ measurements of the CO_2, CO_2 and H_2O were trapped into liquid nitrogen and then cryogenically separated. All values are reported in the delta notation in permil (‰) relative to PDB, with error below 0.2 ‰ (Table 2).

3.3.2 $\delta^{15}N$

Nitrogen isotope measurements were done using the non-condensable fraction of the Giggenbach bottles, which consists mainly of N_2, CO, and noble gases since CO_2 has been removed. Both CO and N_2 gases were transferred in a sealed pyrex tube containing CuO and Cu_2O grains to be oxidized into N2 and CO_2 at 450 ˚C for 1 hour. Prior to being used, the CuO and Cu_2O grains have been heated few minutes under vacuum at 350°C and pumped overnight at room temperature to remove adsorbed gases. The produced CO_2 was then cryogenically trapped and N_2 was collecting using a Toepler pump. All values are reported using the delta notation, in permil (‰) relative to air, with error ~0.5 ‰ calculated from the reproducibility of duplicates (Table 2).

4 Results

4.1 Wells

During the main flow of the SP4 well test, which lasted approximately 10h, samples were collected for $^{3}He/^{4}He$ and $^{4}He/^{20}Ne$ measurements every hour. Sample names follow the format "site name-sampling order + copper tube number" and duplicate samples have an "M1" at the end; sampling order is "100" when before well test, "200" during, and "300" if sampled after the well test (Table 1). For the SP7 well, only one sample was collected for noble gas measurements. SP4 and SP7 are CO_2-dominated, consisting of ~ 94% CO_2 and 6% N_2 and only traces of CH_4 (< 0.6%); helium contents range from 394 to 426 ppm vol. The $\delta^{13}C$ value of the SP4 sample is -10.1 ‰, which is compatible with a primarily organic source of CO_2 or non-marine carbonates (Table 2).

Throughout the SP4 well test, no significant change on helium abundance or isotopic ratios was detected. $^{3}He/^{4}He$ ratios range from 0.17 to 0.21 (± 0.01) R_a, with no temporal variation (Table 2). $^{4}He/^{20}Ne$ ratios are consistently > 2000, however, measurements are not precise due to the low content of ^{20}Ne relative to ^{4}He, with the former showing values very close to the baseline. During the SP7 well test, we only collected one sample, which shows similar results with a $^{3}He/^{4}He$ ratio of 0.18 (± 0.01) Ra and $^{4}He/^{20}Ne > 2000$.

The $^{40}Ar/^{36}Ar$ ratios, measured for two aliquots of the SP4 well gas, are 2866 ± 5 and 2574 ± 11, respectively, with the $^{38}Ar/^{36}Ar$ ratios being indistinguishable from atmosphere (Table 3). The $^{20}Ne/^{22}Ne$ (9.40 ± 0.05) and the $^{21}Ne/^{22}Ne$ ratios (0.0621 ± 0.0011) deviate slightly from the atmospheric Ne value, indicating contribution of crustal (and possibly mantle) neon (see section 5.2). Analyses of SP7 show $^{40}Ar/^{36}Ar$ (696.6 ± 0.2) above the air value, but still lower than the SP4 well, indicating possible atmospheric contamination during drilling operations. Xenon isotopic ratios of SP7 by dynamic mass spectrometry (Table 3) indicate contribution of fissiogenic and mantle Xe (see section 5.2).

4.2 Springs

Fontaines Salées and Bourbon-Lancy are N_2-dominated (93 % and 97 %, respectively) while Fontaine des Vertus is comprised of 63 % CO_2 and 39 % N_2 (Table 1). The remaining springs are CO_2-dominated ranging from 95 to 97 %. For all springs, only traces of CH_4 are identified (< 0.6%). Helium contents range from 245 to

426 ppm vol for the CO_2-dominated sites, and from 2874 to 45794 ppm vol for Fontaine des Vertus, Fontaines Salées, and Bourbon-Lancy.

The springs near SP4 (Gelin, Fonts-Bouillants, and Fontaine des Vertus) present $^3He/^4He$ ratios similar to those of SP4, ranging from 0.16 to 0.21 (± 0.01) R_a, as well as the Pougues-les-Eaux spring which is 25 km north from SP4 (0.22 ± 0.01 R_a) (Table 2). Fontaines Salées and Bourbon-Lancy which are located 80 km NE and 50 km SE of SP4, have distinct $^3He/^4He$ signatures (0.04 ± 0.00 and 0.03 ± 0.00 R_a, respectively) that are close to the purely radiogenic end-member. $^3He/^4He$ variations do not correlate with gas compositions, with similar $^3He/^4He$ for springs near SP4 (including Fontaine des Vertus) despite much higher helium and N_2 contents.

$\delta^{13}C$ of CO_2 values show little variation among the springs, ranging from -11.8 to -10 ‰ (vs. PDB), except for Fontaines Salées (-20 ‰), which suggests either different sources of CO_2 or different processing in the crust. Weinlich (2005) reported comparable values of -13.9 ‰ for a N_2-dominated spring at Pougues-les-Eaux (74 % N_2) and of -20.4 ‰ at Saint Père (94 % N_2), near Fontaines Salées. The Pougues-les-Eaux spring in the present study is dominated by CO_2 (95 vol. %) and has a very similar $\delta^{13}C$ (-10.3 ‰) to the one described in Weinlich (2005). Moreover, the springs with lower CO_2 contents tend to present lighter $\delta^{13}C$ values (Fig. S1) that could indicate chemical processes during transport in the crust due to solution of CO_2 in the water phase and/or carbonate precipitation, concentrating helium and N_2 in the gas phase. $\delta^{15}N$ results for the springs from both groups display similar values (+6.1 to +8.4 ‰) compatible with a primarily crustal source.

5 Discussion

5.1 Source of helium

In European basins of various ages, $^3He/^4He$ values range between 0.01 and 3.9 R_a, reaching ~0.1 R_a in the western Alps (Marty et al., 1992; Oxburgh et al., 1986). Oxburgh et al. (1986) suggested that this wide range in Neogene basins was related to their tectonic setting. Helium isotope compositions in the Pannonian basin reach values up to 3.9 R_a consistent with an extension regimen and clear mantle input while the Molasse and Po basins show a range of $^3He/^4He$ between 0.02 and 0.09 R_a (Marty et al., 1992; Oxburgh et al., 1986), which, for the Molasse basin, Oxburgh et al. (1986) interpret as being of crustal origin despite the apparent small mantle contribution (up to 0.9%). In the Paris Basin, $^3He/^4He$ ratios are close to the range of values for the Molasse

290 and Po basins (0.02 to 0.11 R_a), reaching 0.14 R_a at the basement in Couy (Pinti &
291 Marty, 1998). These values are higher than the theoretical crustal $^3He/^4He$ ratio (0.001-
292 0.02 R_a), based on the U-Th and Li values of the underlying sedimentary rocks. These
293 elevated $^3He/^4He$ values were therefore considered to be evidence for the input of
294 mantle material with a higher than crustal $^3He/^4He$ (Pinti & Marty, 1998). However,
295 with only small $^3He/^4He$ variations, up to 0.1 R_a, it is difficult to fully discriminate this
296 component from variation in the crustal $^3He/^4He$ ratio. In addition, these areas show no
297 evidence of igneous manifestations, and there is the possibility that ^3He could be
298 produced in the crust without mantle input (see section 5.3.1).

299 In the $^3He/^4He$ *versus* $^4He/^{20}Ne$ plot (Fig. 2), we identify two groups of samples:
300 one of them contains Fontaines Salées and Bourbon-Lancy, and the other one contains
301 SP4, SP7, surrounding springs, and Pougues-les-Eaux. Considering the typical values
302 found in the various basins in Europe, the $^3He/^4He$ signature found at Fontaines Salées
303 and Bourbon-Lancy is within the European crustal range (0.02 – 0.1 R_a). The remaining
304 samples show significantly higher $^3He/^4He$ (0.16 – 0.22 R_a). However, in any case, the
305 main source of helium in the basin is from the continental crust.

306 Using U, Th, and Li contents of lithologies from the Paris Basin (Pinti & Marty,
307 1998) (since rock chemistry data is not available for our target area), we calculated the
308 theoretical $^3He/^4He$ signature to be between 0.001 and 0.016 R_a, based on radiogenic
309 (^4He) and nucleogenic (^3He) production equations (Eq. 1; Andrews, 1985). For the SP4
310 sample group that includes SP4, SP7, nearby springs, and Pougues-les-Eaux, we
311 compute that the higher $^3He/^4He$ ratios can either be accounted for by, (i) either
312 nucleogenic ^3He production from the presence of high amounts of lithium in the host
313 rocks, (ii) or by a 2.5 % mantle input to the original crustal signature. In the next
314 sections, we discuss both possibilities for the $^3He/^4He$ signature we find for the SP4
315 group.

316 (Eq. 1) $$P_3/P_4 = f(R, Na, Mg, Al, Si, Ca)F_{Li}/(3.2108\ x\ 10^6 + 7.7633\ x\ 10^5 R)$$

317 Where P_3/P_4 is the theoretical $^3He/^4He$ based on the ^3He and ^4He production
318 rates, $f(...)$ is the neutron production rate based on the composition, F_{Li} is the fraction of
319 neutrons that are captured by ^6Li in the rock matrix, and R is the Th/U ratio.

5.1.1 *Nucleogenic ^{3}He production*

As previously stated, one potential production pathway to increase the $^3He/^4He$ from crustal values to that measured in the SP4, SP7, surrounding springs, and Pougues-les-Eaux samples is through the localised production of nucleogenic helium (^3He) via thermal neutron capture on ^6Li via the reaction $^6Li(n,\alpha)^3H\ (\beta^-) \rightarrow {}^3He$ (Morrison & Pine, 1955). To raise the $^3He/^4He$ signatures of the SP4 sample group (Fig. 2, Table 2) from an assumed original crustal signature (0.001 – 0.016 R_a) we calculate that it would require Li concentrations in the basement and/or host rocks to be on the order of 600 ppm (Andrews, 1985; Eq. 1). This calculation assumes that all the excess ^3He within the samples is produced from the thermal neutron capture by ^6Li and that the basement / host rock contains typical crustal U-Th concentrations (1.8 and 7.2 ppm, respectively; Krauskopf and Bird, 1967). Although this amount of Li is atypical in view of the average continental crust value (30 ppm Li), small proximal basins such as the ones in the Massif Central have the potential to accumulate lithium (Sun et al., 2022).

One of the major concentrated sources of lithium in the crust is surface and subsurface brines. Near the study region (~ 100 km), in the Massif Central, a geothermal brine with 81 ppm Li has been identified in the Limagne basin (Fonroche geothermie, 2019) but values higher than that have not yet been reported. Brines from the area were previously described with much lower lithium contents (e.g., Millot et al., 2007; 7 ppm). In the Paris Basin, lithium concentration is low, in brines associated with Triassic salt deposits (up to 60 ppm; Fontes & Matray, 1993a; Millot et al., 2011) and oil fields (4.8 ppm; Fontes & Matray, 1993b b).

Apart from brines and geothermal water, the main *hard-rocks* that are sources of lithium are rare-metal-rich granites such as the Beauvoir, Montebras, and Chavence granites, near our study area, LCT pegmatites, and greisen deposits produced by high-temperature hydrothermal alteration of the aforementioned types (Gourcerol et al., 2019). The lithium mineralizations in the Massif Central are usually located near important ductile faults (Gloaguen et al., 2018).

Considering the various sources of lithium with production potential (Gloaguen et al., 2018) in the Massif Central, near the study area, it is possible to consider that a Li-rich granitic basement produces significant quantities of helium. The closest lithium sources are the Chavence (56 km SE) and Beauvoir granites (72 km SW), the latter

containing lithium concentrations between 367 and 5,220 ppm in its upper units (Raimbault et al., 1995). Taking the U, Th, and Li contents from the Beauvoir granite (16.2 - 52.4, 1.15 - 5.63, and 367 - 5,220 ppm, respectively; Raimbault et al., 1995), the theoretical $^{3}He/^{4}He$ ratios would range between 0.12 and 1.66 R_a. In that case, helium could be produced in the basement, before migrating upwards to the basin and being stored in the sedimentary layers, acting as a reservoir. Another possibility is that, as a proximal basin, detrital material from the Li-rich rocks accumulates in the basin and ^{3}He is produced in the sedimentary layers. The Chavence granite is located near Bourbon-Lancy (~ 9 km) where we find a crustal signature for helium isotopes; however, at Bourbon-Lancy, the spring is directly on top of the basement and not in a sedimentary basin. To observe the same signatures as for the SP4 sample group at Bourbon-Lancy, a sedimentary basin that accumulates and traps the produced gas is required, as otherwise degassing from a Li-rich source would only occur locally and relatively far from the spring. There are also non-conventional sources of lithium that have recently been brought to light and that cannot be discarded, such as coal (e.g., Qin et al., 2015). Considering the regional geology, Stephanian-Permian basins in the Massif Central region have coal levels (Mercuzot et al., 2021) that could potentially provide the required amounts of lithium.

In the context of local production, Martel et al. (1990) found $^{3}He/^{4}He$ ratios (0.025 R_a) higher than the expected theoretical value (0.0033 R_a) for the Carnmenellis granite-hosted water (England). They explain this observation by presenting a model of preferential release of ^{3}He from the rocks, relative to ^{4}He. However, this model only works if some conditions are satisfied to retain ^{4}He within the minerals – i.e., U and Th get concentrated in accessory phases and the host rock has remained at low temperature since formation (hence limiting He loss through diffusion). In our current study, testing this model would require detailed mineralogical characterization, but currently the composition of underlying basement and host rock is not well known Furthermore, the Paris Basin has a relatively high heat flux (60 to 120 mW/m2; Dentzer et al., 2016; Torgersen, 1993) which makes this model unlikely.

5.1.2 Mantle contribution

The alternative explanation for $^{3}He/^{4}He$ ratios above typical crustal values is a contribution of mantle-derived ^{3}He. This could originate from an old magmatic source

384 in the crust, put in place around the time of basin formation, or from more recent
385 magma intrusions.

386 Méjean et al. (2020) proposed a model in which a fossil magmatic signal is
387 diluted over time by radiogenic ^{4}He production in the crust. This model is appropriate to
388 explain the mantle input observed in the Southern Quebec groundwater since a clear
389 alignment of Cretaceous magmatic intrusions is present (Monteregian Hills Igneous
390 Province). For the Paris Basin, however, no evidence of magma emplacement in such
391 scale during its formation is found.

392 Pinti and Marty (1998) describe two possibilities for the minor mantle signature in
393 the Paris Basin observed in He isotopes – either from Permo-Carboniferous intrusions
394 in Couy (lamprophyre dykes) or from a deep-seated magmatic source. The former could
395 explain localized variations in the $^{3}He/^{4}He$ ratios but is unlikely to explain the
396 signatures observed across a broad area. Furthermore, if the mantle input was coming
397 from magmatic bodies that have already crystallized, helium would need to be liberated
398 from minerals. For such a process to happen, certain temperatures must be reached to
399 release He from the mineral; in the case of olivine crystals, helium release from fluid
400 inclusions seems to start at ~ 500°C (Tolstikhin et al., 2010) while closure temperatures
401 are between 143 and 244°C (Shuster et al., 2004; Wang et al., 2015). In this case,
402 diffusion is the primary process, and will not only depend on the current isotherms but
403 also on the age of the crystallized body. Furthermore, cooling rates may play a role in
404 controlling the availability of He since, if the heat flux has been continuously high in
405 the region and the minerals crystallized long ago, the majority of the helium would
406 likely have been lost from the magmatic body. A deep-seated magmatic source could
407 explain the vertical $^{3}He/^{4}He$ gradient observed (Marty et al., 1993; Pinti & Marty, 1998)
408 from the basement-hosted groundwater with 0.12-0.14 R_a, going through the Triassic
409 aquifer with 0.08 R_a, and terminating at the Middle Jurassic waters at 0.02 R_a.

410 In Fig. 3, we observe a geographical trend with $^{3}He/^{4}He$ decreasing from the
411 South (Massif Central) towards the north (Paris Basin) while the SP4 sample group
412 shows intermediate $^{3}He/^{4}He$ ratios. Considering that this trend coincides with the N-S
413 orientation of the fault systems, it could point to a localized weakening of the crust that
414 facilitates mantle input by degassing of a melt generated by decompression and partial
415 melting. The horizontal transport of gases with a mantle signature from a relatively
416 young magmatic system through faults is unlikely since the most recent active volcanic

system in the region is located in the Chaîne des Puys (4040 BCE), 90 km south of our study area in the Massif Central (2.9- 3.2 Ra; Bräuer et al., 2017). Also, no evidence for transport of gas via groundwater is observed in the dataset: transport through large distances would entail gas-water interaction and the $^{4}He/^{20}Ne$ ratios are consistently above 2000 and far from the air-saturated water value (~ 0.28). For the eastern segment of the Paris Basin, further from our study area in the Lorraine region, Marty et al. (2003) proposed that the elevated signatures (0.4 R_a) might originate from nearby rifting in the Rhine graben (1.7 Ra; Griesshaber et al., 1992), which is up to 120 km away from their studied sites. Similarly, for the Drôme County, in the subalpine massifs (SE France), $^{3}He/^{4}He$ ratios have a wide range and can reach relatively high values (0.02 to 3.64 Ra; Marty et al., 1992) while being ~ 70 km away from the nearest volcanic systems (Ardèche and Auvergne). In both studies, $^{4}He/^{20}Ne$ and $^{3}He/^{4}He$ ratios of groundwater samples plot along a mixing line between ASW and a crust/mantle component and thus water could work as the transport medium of the magmatic $^{3}He/^{4}He$ component.

The input of mantle ^{3}He in some of our sample sites may therefore come directly from the mantle underlying the continental crust. In the Pannonian basin and Rhine graben, the crustal thickness is low, around 25 km and heat flow is on the order of 80 mW/m^2 (Čermák, 1982). Similarly, the current crustal thickness of the Paris Basin varies between 29 and 41 km (Lefort & Agarwal, 1996; Prijac et al., 2000) while the heat flux is between 60 and 120 mW/m2 (Dentzer et al., 2016; Torgersen, 1993). However, in the Morvan, the crustal thickness is lower at between 27 and 29 km (Lefort & Agarwal, 1996) despite the typical crustal $^{3}He/^{4}He$ signatures (up to 0.04 R_a; current study). This suggests that crustal thickness and diffusive transport of mantle material through the crust is unlikely to be the dominant source of mantle ^{3}He within these systems. Therefore, Marty et al. (1993) interpret the anomalous $^{3}He/^{4}He$ signatures as the result of degassing of partial melts at depth, which explains the vertical ^{3}He flux.

Although the commonly known processes by which mantle helium enters the crust are via magmatic intrusions, degassing of magma, or diffusion, in areas without recent volcanism and under either extension or compression regimes, mantle input can also occur via advective flow controlled by faults due to improved permeability (Kennedy & van Soest, 2007; Kulongoski et al., 2005, 2013). In the model proposed by Kennedy & van Soest (2007), a vertical fault splay must penetrate the ductile lower

crust and reach the mantle acting as a channel for fluid flow. To satisfy this model, strain localization must occur to generate vertical faults in depth; Kennedy & van Soest (2007) propose this process is possible with increased dextral shear strain. The areas where mantle input via advective flow have been described (Kennedy & van Soest, 2007; Kulongoski et al., 2005, 2013) are seismically active regions, however, which is not the case for the Paris Basin. Slow deforming areas can present seismicity such as in the Armorican Massif or the Massif Central, west and south of the Paris Basin, respectively; the main difference between them, in a tectonic context, is the presence of a thick unfaulted Meso-Cenozoic sedimentary pile that acts as a "patch" and protects the basement rocks in the Paris Basin from brittle movement by improving the cohesion and decreasing the thickness of the breakable portion of the upper crust (Petit et al., 2019). Our study area, nonetheless, is at the border of the basin and contains a series of faults. Further South, closer to the Massif Central, earthquakes with magnitudes up to M4.4 have been recorded (Mazabraud et al., 2005). The closest to the study area (~ 40 km south) was an M4.1 in 1977, near Vieure (46.52°N, 2.93°E; Mazabraud et al., 2005). To test if mantle input occurs via advective flow controlled by faults, a detailed structural and geophysical study of the region is necessary.

In any case, the anomalous $^{3}He/^{4}He$ signatures – above typical crustal values for this part of the crust – seem to be focused along the N-S fault systems with an apparent decreasing gradient starting at the Massif Central volcanic area up to the Paris Basin. This trend, coupled with the vertical $^{3}He/^{4}He$ gradient observed at the Paris Basin $^{3}He/^{4}He$ (Marty et al., 1993; Pinti & Marty, 1998), seem to point to a localized and limited mantle input along these faults, which is endorsed by the ^{129}Xe excess observed at SP7 (see section 5.2).

5.2 Ar, Ne, and Xe isotope constraints

The Ne isotopic signature of SP4 is dominated by a nucleogenic production within the continental crust, however, the data point lies slightly above the typical crust-air mixing line (Fig 4), which could be due to either (i) simple two component mixing between air and a Ne endmember between modern crustal values and Archean terrains, or (ii) a limited contribution of mantle Ne to crustal and atmospheric Ne. The fact that there is only a single data point does not allow us to draw mixing line(s) and therefore precludes a definitive conclusion about a possible contribution of mantle Ne.

The argon isotopic composition of SP4 gas (Table 3) indicates either atmospheric or mantle origin for the $^{38}Ar/^{36}Ar$ ratio and a significant contribution of radiogenic ^{40}Ar produced by the decay of ^{40}K over long periods of time ($T_{1/2}$ = 1.25 Ga). Indeed, the $^{40}Ar/^{36}Ar$ ratios of 2866 are one order of magnitude higher than the atmospheric value of 298.6. High $^{40}Ar/^{36}Ar$ values are observed in both crustal and mantle rocks and gases, so it is not possible a priori to decipher the origin of such radiogenic Ar, but the continental environment of the gas reservoir and the low $^{3}He/^{4}He$ ratio compared to typical mantle He values suggests a strong crustal contribution.

At the level of ultra-high precision provided by dynamic mass spectrometry, the isotopic composition of SP7 xenon is shown to deviate from that of atmospheric Xe. High precision Xe analysis from SP7 (Fig 5) shows a small yet distinguishable ^{129}Xe excess (relative to the atmosphere). ^{129}Xe excess is linked to ^{129}I decay either by ^{238}U spontaneous fission, cosmogenic origin, or trapped in the mantle reservoir from production in the first ~ 100 Myr of the Earth formation (Moreira, 2013; Mukhopadhyay & Parai, 2019). Although ^{129}Xe can be produced in the crust by ^{129}I decay from ^{238}U spontaneous fission, considering the $^{136}Xe/^{130}Xe$ is very low (corrected absolute ratio of 2.207) and the upper limit for $^{129}Xe/^{136}Xe$ of ^{238}U-fissiogenic Xe is 0.001 (Eikenberg et al., 1993), the $^{129}Xe/^{130}Xe$ originated from fissiogenic ^{238}U would be minimal (< 1%).

Cosmogenic ^{129}I is concentrated in sediments enriched in carbon (Santos et al., 2007); Holland et al. (2013) attributed the ^{129}Xe observed in the Timmins mine fluids to cosmogenic ^{129}I due to the age of the host rocks/fluids (Archean), presence of carbon-rich sediments, and absence of any evidence for mantle input since the $^{3}He/^{4}He$ ratios were within typical crustal ranges (up to 0.01 R_a). As discussed in section 5.1.1, Stephanian-Permian basins in the Massif Central region have coal levels (Mercuzot et al., 2021), however, the geology of the basin of our current study is not yet well established. Thus, in our study area, considering the helium isotope signature above typical crustal values (up to 0.22 R_a), ^{129}Xe excess is linked to mantle input.

Notably, heavy Xe isotopes are clearly enriched relative to the lighter ones (e.g., ^{130}Xe). Such enrichment is likely to result from the contribution of fissiogenic Xe due to the spontaneous fission of long-lived ^{238}U (Mukhopadhyay & Parai, 2019). Thus, the isotopic composition of xenon confirms that SP7 hosts gas components derived from both the mantle and crust.

5.3 *CO_2/^{3}He and stable isotope constraints*

The overall $\delta^{13}C$ of CO_2 signatures are outside the MORB range (-5 ± 2 ‰) and within range of non-marine carbonates, graphite, and marine plants (Favara et al., 2002). However, for the SP4 group, with exception of Fontaine des Vertus, $CO_2/^3He$ is close to the MORB values (~ 1 to 6 x 10^9; Marty & Zimmermann, 1999), ranging from 8 x 10^9 to 1 x 10^{10}. In a $CO_2/^3He$ versus $\delta^{13}C$ plot (Sano and Marty, 1995; Fig. 6), the CO_2-dominated samples show a mixing between three components, namely mid-ocean ridge basalts (MORB), organic sediments, and marine limestones (or slab carbonates). Considering that ^3He is mainly of mantle origin, the end-member contributions would range from 15 % to 30 % MORB, 40 % to 55 % limestones, and 25% to 30 % sediments contribution to the source of CO_2. Secondary processes can still play an important role in the CO_2 and $\delta^{13}C$ values (Supplementary material); Gilfillan et al (2009) propose that $CO_2/^3He$ variations in different gas fields are due to CO_2 loss either from dissolution in groundwater or carbonate precipitation, and that the $\delta^{13}C$ will vary according to the water pH in a negative correlation (Randazzo et al., 2021).

In the Massif Central, $\delta^{13}C$ varies between -6.3 ‰ and -3.6 ‰ while $CO_2/^3He$ ranges from 3.9 x 10^9 to 1 x 10^{13} (Bräuer et al., 2017), which falls between upper mantle and marine limestone in Fig. 6. This range can be interpreted as representing the composition of the typical regional mantle end-member. In this case, we might observe, for the SP4 group, the occurrence of a mantle-like component associated with CO_2 dissolution in water leading to more depleted $\delta^{13}C$ or a small contribution from organic sediments, and at Fontaines Salées and Bourbon-Lancy, an organic source. Alternatively, CO_2 in the SP4 group samples might originate from non-marine carbonates or graphite which can range, respectively, from ~ -18 ‰ to 0 ‰ and ~ -40 ‰ to 0 ‰ (Favara et al., 2002) that can still be associated with mixing with a MORB component. The history of CO_2 transport might be more complex for Fontaines Salées and Bourbon-Lancy and could reflect secondary processes.

CO_2 reservoirs worldwide are generally interpreted as being magmatic in origin, with $\delta^{13}C$ ranging between - 5.7 to – 2.7 ‰ (Gilfillan et al., 2009); compared to them our dataset is atypical. However, in such reservoirs, water is the storage medium of CO_2 (Dubacq et al., 2012; Gilfillan et al., 2008) while in our study we did not identify water bodies at depth and no water manifested during the well tests. Nonetheless, in areas with no evidence of volcanism, CO_2 flow in the surface has already been reported for

seismically active areas (e.g. Li Vigni et al., 2022), indicating that fault systems can lead to complex histories of CO_2 transport and entrapment.

For all samples, the $\delta^{15}N$ values show little variation, ranging from +6.1 to +8.4 ‰. This range is typical of continental or subduction-related gases and differs from that of MORB (around -5 ‰ in the convecting mantle; Marty & Dauphas, 2003). Mantle plumes also show lower $\delta^{15}N$ values, around 0 ± 3 ‰ (Labidi et al., 2020; Marty & Dauphas, 2003). In the Massif Central, $\delta^{15}N$ values around +2 ‰ (Bräuer et al., 2017) could potentially indicate the presence of a mantle plume or, alternatively, mixing between MORB-like and continental-like components. The near-constant $\delta^{15}N$ values of the present samples point to a common nitrogen source despite large variations in the N_2 contents of the surveyed springs. Such variable N_2 contents might be relative to secondary physical/chemical processes in the crust since higher contents of N_2 and helium are associated with more depleted $\delta^{13}C$ values (Fig S1).

6 Conclusion

The main source of helium in the study area is the continental crust. $^3He/^4He$ ratios are independent of gas composition, given that $^3He/^4He$ is roughly the same for springs near SP4, including Fontaine des Vertus, while its helium and N_2 contents are much higher than for the other springs of the group. Local helium production alone is unlikely since the $^3He/^4He$ ratios (0.17-0.22 R_a) are in the same range across a 40 km area (Pougues-les-Eaux and Couy). To verify if ^3He and ^4He are produced and stored in the reservoir layers or if they are transported from a crustal flux, the U-Th-Li contents of the host rocks of the sites investigated is required, and a better understanding of the basin geometry and sources is necessary.

The decreasing $^3He/^4He$ gradient starting at the Massif Central towards the Paris Basin and the vertical $^3He/^4He$ gradient previously described in the literature at the Paris Basin aquifers (Marty et al., 1993; Pinti & Marty, 1995, 1998) point to a small mantle contribution limited to the N-S fault system, since laterally, few kilometres (50-80) east at Bourbon-Lancy and Fontaines Salées, $^3He/^4He$ ratios show typical crustal values (≤ 0.04 R_a). The ^{129}Xe excess observed at SP7 confirms that excess ^3He relative to the crustal end-member composition is derived from the mantle. This indicates that either a

deep-seated magmatic source is present, or deep fault systems reach the mantle and input ^{3}He via an improved permeability system (Kennedy & van Soest, 2007).

Considering that the $\delta^{13}C$ of CO_2 of our surveyed springs are distinct from the regional mantle value (Massif Central), CO_2 is probably mainly of crustal origin. However, mixing between crustal or biogenic components and mantle is expected, especially since CO_2 would most likely be the carrier phase of the mantle helium component and $CO_2/^{3}He$ ratios (between 8×10^{9} and 1×10^{10}) are close to the MORB value and indicate a ~ 15% mantle contribution, in agreement with what is observed in He and Xe isotopes. Secondary processes in the crust are also possible given the low solubility of CO_2 in water, and potential carbonate precipitation can also explain the decrease of CO_2 contents associated with elevated concentrations of N_2 and helium at Fontaine des Vertus, Bourbon-Lancy, and Fontaines Salées. $\delta^{15}N$ results, for both sample groups, are comparable and point to a common crustal source.

ACKNOWLEDGEMENTS

We thank A. Caracausi for the insightful discussions. We are also thankful to L. Zimmermann and B. Tibari for helping with the analyses. We gratefully thank the two anonymous reviewers of this article and the Editor for his handling of our manuscript. This work was partially supported by the French PIA project "Lorraine Université d'Excellence", reference ANR-15-IDEX-04-LUE. This is CRPG contribution # ?

REFERENCES

Andrews, J. N. (1985). The isotopic composition of radiogenic helium and its use to study groundwater movement in confined aquifers. *Chemical Geology*, *49*(1–3), 339–351. https://doi.org/10.1016/0009-2541(85)90166-4

Ballentine, C. J., & Burnard, P. G. (2002). Production, release and transport of noble gases in the continental crust. *Reviews in Mineralogy and Geochemistry*, *47*. https://doi.org/10.2138/rmg.2002.47.12

Baptiste, J. (2016). *Cartographie structurale et lithologique du substratum du Bassin parisien et sa place dans la chaîne varisque de l'Europe de l'Ouest: approches combinées géophysiques, pétrophysiques, géochronologiques et modélisations 2D*. Université d'Orléans.

Barruol, G., & Granet, M. (2002). A Tertiary asthenospheric flow beneath the southern French Massif Central indicated by upper mantle seismic anisotropy and related to the west Mediterranean extension. *Earth and Planetary Science Letters*, *202*(1), 31–47.

Batard, F., Baubron, J. C., Bosch, B., Marcé, A., & Risler, J. J. (1982). Isotopic identification of gases of a deep origin in French thermomineral waters. *Journal of Hydrology*, *56*(1–2), 1–21. https://doi.org/10.1016/0022-1694(82)90053-1

Battani, A., Deville, E., Faure, J. L., Jeandel, E., Noirez, S., Tocqué, E., Benoît, Y., Schmitz, J., Parlouar, D., & Sarda, P. (2010). Geochemical study of natural CO2 emissions in the French Massif Central: how to predict origin, processes and evolution of CO2 leakage. *Oil & Gas Science and Technology–Revue de l'Institut Français Du Pétrole*, *65*(4), 615–633.

Beccaletto, L., Capar, L., Serrano, O., & Marc, S. (2015). Structural evolution and sedimentary record of the Stephano-Permian basins occurring beneath the Mesozoic sedimentary cover in the southwestern Paris basin (France). *Bulletin de La Societe Geologique de France*, *186*(6), 429–450. https://doi.org/10.2113/gssgfbull.186.6.429

Bekaert, D. V, Barry, P. H., Broadley, M. W., Byrne, D. J., Marty, B., Ramírez, C. J., de Moor, J. M., Rodriguez, A., Hudak, M. R., & Subhas, A. V. (2023). Ultrahigh-precision noble gas isotope analyses reveal pervasive subsurface fractionation in hydrothermal systems. *Science Advances*, *9*(15), eadg2566.

Bekaert, D. v, Broadley, M. W., Caracausi, A., & Marty, B. (2019). Novel insights into the degassing history of Earth's mantle from high precision noble gas analysis of magmatic gas. *Earth and Planetary Science Letters*, *525*, 115766.

Boineau, R., & Maisonneuve, J. (1972). Les sources minérales du Massif Central français et leur cadre géologique. *Rapport BRGM*.

Bräuer, K., Kämpf, H., Niedermann, S., & Wetzel, H. U. (2017). Regional distribution pattern of carbon and helium isotopes from different volcanic fields in the French Massif Central: Evidence for active mantle degassing and water transport. *Chemical Geology*, *469*(February), 4–18. https://doi.org/10.1016/j.chemgeo.2017.04.004

Broadley, M. W., Barry, P. H., Bekaert, D. v, Byrne, D. J., Caracausi, A., Ballentine, C. J., & Marty, B. (2020). Identification of chondritic krypton and xenon in Yellowstone gases and the timing of terrestrial volatile accretion. *Proceedings of the National Academy of Sciences*, *117*(25), 13997–14004.

Broadley, M. W., Byrne, D. J., Ardoin, L., Almayrac, M. G., Bekaert, D. v, & Marty, B. (2022). High precision noble gas measurements of hydrothermal quartz reveal variable loss rate of Xe from the Archean atmosphere. *Earth and Planetary Science Letters*, *588*, 117577. https://doi.org/https://doi.org/10.1016/j.epsl.2022.117577

Buikin, A., Trieloff, M., Hopp, J., Althaus, T., Korochantseva, E., Schwarz, W. H., & Altherr, R. (2005). Noble gas isotopes suggest deep mantle plume source of late Cenozoic mafic alkaline volcanism in Europe. *Earth and Planetary Science Letters*, *230*(1–2), 143–162.

Čermák, V. (1982). Crustal temperature and mantle heat flow in Europe. *Tectonophysics*, *83*(1–2), 123–142. https://doi.org/10.1016/0040-1951(82)90012-9

Clozier, L., & Turland, M. (1982). *Notice explicative de la feuille Dornes a 1/50 000*.

Coisy, P., & Nicolas, A. (1978). Regional structure and geodynamics of the upper mantle beneath the Massif Central. *Nature*, *274*(5670), 429–432.

Craig, H., & Lupton, J. E. (1976). Primordial neon, helium, and hydrogen in oceanic basalts. *Earth and Planetary Science Letters*, *31*(3), 369–385.

Dentzer, J., Lopez, S., Violette, S., & Bruel, D. (2016). Quantification of the impact of paleoclimates on the deep heat flux of the Paris Basin.

Geothermics, *61*, 35–45. https://doi.org/10.1016/j.geothermics.2016.01.006

Dubacq, B., Bickle, M. J., Wigley, M., Kampman, N., Ballentine, C. J., & Sherwood Lollar, B. (2012). Noble gas and carbon isotopic evidence for CO 2-driven silicate dissolution in a recent natural CO 2 field. *Earth and Planetary Science Letters*, *341–344*, 10–19. https://doi.org/10.1016/j.epsl.2012.05.040

Eikenberg, J., Signer, P., & Wieler, R. (1993). U-Xe, U-Kr, and U-Pb systematics for dating uranium minerals and investigations of the production of nucleogenic neon and argon. *Geochimica et Cosmochimica Acta*, *57*(5), 1053–1069. https://doi.org/https://doi.org/10.1016/0016-7037(93)90040-4

Farjanel, G. (1989). *Synthèse géologique des bassins permiens français* (Issue 128). Editions BRGM.

Favara, R., Grassa, F., Inguaggiato, S., Pecoraino, G., & Capasso, G. (2002). A simple method to determine the δ13C content of total dissolved inorganic carbon. *Geofisica Internacional*, *41*(3), 313–320.

Fonroche geothermie. (2019). *Notice Technique du PER dit de "Bassin de Limagne."* https://www.economie.gouv.fr/files/files/PDF/2020/D_Notice_impact_PER_Limagne.pdf

Fontes, J. C., & Matray, J. M. (1993a). Geochemistry and origin of formation brines from the Paris Basin, France. 1. Brines associated with Triassic salts. *Chemical Geology*, *109*(1–4), 149–175. https://doi.org/10.1016/0009-2541(93)90068-T

Fontes, J. Ch., & Matray, J. M. (1993b). Geochemistry and origin of formation brines from the Paris Basin, France: 2. Saline solutions associated with oil fields. *Chemical Geology*, *109*(1), 177–200. https://doi.org/https://doi.org/10.1016/0009-2541(93)90069-U

Froidevaux, C., Brousse, R., & Bellon, H. (1974). Hot spot in France? *Nature*, *248*(5451), 749–751.

Gautheron, C., Moreira, M., & Allègre, C. (2005). He, Ne and Ar composition of the European lithospheric mantle. *Chemical Geology*, *217*(1–2), 97–112.

Giggenbach, W. F., & Goguel, R. L. (1988). *Methods for the collection and analysis of geothermal and volcanic water and gas samples*. Chemistry Division, Department of Scientific and Industrial Research.

Gilfillan, S. M. V., Ballentine, C. J., Holland, G., Blagburn, D., Lollar, B. S., Stevens, S., Schoell, M., & Cassidy, M. (2008). The noble gas geochemistry of natural CO2 gas reservoirs from the Colorado Plateau and Rocky Mountain provinces, USA. *Geochimica et Cosmochimica Acta*, *72*(4), 1174–1198. https://doi.org/10.1016/j.gca.2007.10.009

Gilfillan, S. M. V., Lollar, B. S., Holland, G., Blagburn, D., Stevens, S., Schoell, M., Cassidy, M., Ding, Z., Zhou, Z., Lacrampe-Couloume, G., & Ballentine, C. J. (2009). Solubility trapping in formation water as dominant CO2 sink in natural gas fields. *Nature*, *458*(7238), 614–618. https://doi.org/10.1038/nature07852

Gloaguen, E., Melleton, J., Lefebvre, G., Tourière, B., Yart, S., & Gourcerol, B. (2018). *Ressources métropolitaines en lithium et analyse du potentiel par méthodes de prédictivité*. Public report BRGM/RP-68321-FR, 126p. http://infoterre. brgm. fr/rapports/RP ….

Glueckauf, E. (1946). A micro-analysis of the helium and neon contents of air. *Proceedings of the Royal Society of London. Series A. Mathematical and Physical Sciences*, *185*(1000), 98–119.

Gourcerol, B., Gloaguen, E., Melleton, J., Tuduri, J., & Galiegue, X. (2019). Re-assessing the European lithium resource potential – A review of hard-rock resources and metallogeny. *Ore Geology Reviews*, *109*(April), 494–519. https://doi.org/10.1016/j.oregeorev.2019.04.015

Graham, D. W. (2002). Noble gas isotope geochemistry of mid-ocean ridge and ocean island basalts: Characterization of mantle source reservoirs. *Reviews in Mineralogy and Geochemistry*, *47*, 247–317. https://doi.org/10.2138/rmg.2002.47.8

Griesshaber, E., O'Nions, R. K., & Oxburgh, E. R. (1992). Helium and carbon isotope systematics in crustal fluids from the Eifel, the Rhine Graben and Black Forest, F.R.G. *Chemical Geology*, *99*(4), 213–235. https://doi.org/10.1016/0009-2541(92)90178-8

Guillocheau, F., Robin, C., Allemand, P., Bourquin, S., Brault, N., Dromart, G., Friedenberg, R., Garcia, J.-P., Gaulier, J.-M., & Gaumet, F. (2000). Meso-Cenozoic geodynamic evolution of the Paris Basin: 3D stratigraphic constraints. *Geodinamica Acta*, *13*(4), 189–245.

Holland, G., Lollar, B. S., Li, L., Lacrampe-Couloume, G., Slater, G. F., & Ballentine, C. J. (2013). Deep fracture fluids isolated in the crust since the Precambrian era. *Nature*, *497*(7449), 357–360. https://doi.org/10.1038/nature12127

Jolivet, L., Baudin, T., Calassou, S., Chevrot, S., Ford, M., Issautier, B., Lasseur, E., Masini, E., Manatschal, G., & Mouthereau, F. (2021). Geodynamic evolution of a wide plate boundary in the Western Mediterranean, near-field versus far-field interactions. *BSGF-Earth Sciences Bulletin*, *192*(1), 48.

Joly, A. (2007). *Relations plutons et discontinuités lithosphériques: approche pluridisciplinaire de la mise en place de plutons granitiques le long du Sillon Houiller (Massif Central Français): apports des études de terrain et des données gravimétriques, magnétiques et A*. Orléans.

Kennedy, B. M., & van Soest, M. C. (2007). Flow of mantle fluids through the ductile lower crust: Helium isotope trends. *Science*, *318*(5855), 1433–1436. https://doi.org/10.1126/science.1147537

Krauskopf, K. B., & Bird, D. K. (1967). *Introduction to geochemistry* (Vol. 721). McGraw-Hill New York.

Kulongoski, J. T., Hilton, D. R., Barry, P. H., Esser, B. K., Hillegonds, D., & Belitz, K. (2013). Volatile fluxes through the Big Bend section of the San Andreas Fault, California: Helium and carbon-dioxide systematics. *Chemical Geology*, *339*, 92–102. https://doi.org/10.1016/j.chemgeo.2012.09.007

763 Kulongoski, J. T., Hilton, D. R., & Izbicki, J. A. (2005). Source and
764 movement of helium in the eastern Morongo groundwater Basin: The
765 influence of regional tectonics on crustal and mantle helium fluxes.
766 *Geochimica et Cosmochimica Acta*, *69*(15), 3857–3872.
767 https://doi.org/10.1016/j.gca.2005.03.001

768 Labidi, J., Barry, P. H., Bekaert, D. v., Broadley, M. W., Marty, B., Giunta,
769 T., Warr, O., Sherwood Lollar, B., Fischer, T. P., Avice, G., Caracausi,
770 A., Ballentine, C. J., Halldórsson, S. A., Stefánsson, A., Kurz, M. D.,
771 Kohl, I. E., & Young, E. D. (2020). Hydrothermal 15N15N abundances
772 constrain the origins of mantle nitrogen. *Nature*, *580*(7803), 367–371.
773 https://doi.org/10.1038/s41586-020-2173-4

774 Lefort, J. P., & Agarwal, B. N. P. (1996). Gravity evidence for an Alpine
775 buckling of the crust beneath the Paris Basin. *Tectonophysics*, *258*(1–4),
776 1–14. https://doi.org/10.1016/0040-1951(95)00148-4

777 Li Vigni, L., Cardellini, C., Temovski, M., Ionescu, A., Molnár, K., Palcsu,
778 L., Gagliano, A. L., Cappuzzo, S., & D'Alessandro, W. (2022). Duvalo
779 "Volcano" (North Macedonia): A Purely Tectonic-Related CO2
780 Degassing System. *Geochemistry, Geophysics, Geosystems*, *23*(4).
781 https://doi.org/10.1029/2021GC010198

782 Mabry, J., Lan, T., Burnard, P., & Marty, B. (2013). High-precision helium
783 isotope measurements in air. *Journal of Analytical Atomic Spectrometry*,
784 *28*(12), 1903–1910. https://doi.org/10.1039/c3ja50155h

785 Manatschal, G., Chenin, P., Lescoutre, R., Miró, J., Cadenas, P., Saspiturry,
786 N., Masini, E., Chevrot, S., Ford, M., & Jolivet, L. (2021). The role of
787 inheritance in forming rifts and rifted margins and building collisional
788 orogens: a Biscay-Pyrenean perspective. *BSGF-Earth Sciences Bulletin*,
789 *192*(1), 55.

790 Martel, D. J., O'Nions, R. K., Hilton, D. R., & Oxburgh, E. R. (1990). The
791 role of element distribution in production and release of radiogenic
792 helium: the Carnmenellis Granite, southwest England. *Chemical*

Geology, *88*(3–4), 207–221. https://doi.org/10.1016/0009-2541(90)90090-T

Marty, B., & Dauphas, N. (2003). The nitrogen record for crust-mantle interaction and mantle convection from Archean to Present. *Earth and Planetary Science Letters*, *206*(3–4), 397–410. https://doi.org/10.1016/S0012-821X(02)01108-1

Marty, B., Dewonck, S., & France-Lanord, C. (2003). Geochemical evidence for efficient aquifer isolation over geological timeframes. *Nature*, *425*(6953), 55–58. https://doi.org/10.1038/nature01966

Marty, B., O'Nions, R. K., Oxburgh, E. R., Martel, D., & Lombardi, S. (1992). Helium isotopes in Alpine regions. *Tectonophysics*, *206*(1–2), 71–78. https://doi.org/10.1016/0040-1951(92)90368-G

Marty, B., Torgersen, T., Meynier, V., O'Nions, R. K., & de Marsily, G. (1993). Helium isotope fluxes and groundwater ages in the Dogger Aquifer, Paris Basin. *Water Resources Research*, *29*(4), 1025–1035.

Marty, B., & Zimmermann, L. (1999). Volatiles (He, C, N, Ar) in mid-ocean ridge basalts: Assesment of shallow-level fractionation and characterization of source composition. *Geochimica et Cosmochimica Acta*, *63*(21), 3619–3633. https://doi.org/10.1016/S0016-7037(99)00169-6

Mazabraud, Y., Béthoux, N., & Deroussi, S. (2005). Characterisation of the seismological pattern in a slowly deforming intraplate region: Central and western France. *Tectonophysics*, *409*(1–4), 175–192. https://doi.org/10.1016/j.tecto.2005.08.021

McKinney, C. R., McCrea, J. M., Epstein, S., Allen, H. A., & Urey, H. C. (1950). Improvements in mass spectrometers for the measurement of small differences in isotope abundance ratios. *Review of Scientific Instruments*, *21*(8), 724–730.

Méjean, P., Pinti, D. L., Kagoshima, T., Roulleau, E., Demarets, L., Poirier, A., Takahata, N., Sano, Y., & Larocque, M. (2020). Mantle helium in

Southern Quebec groundwater: A possible fossil record of the New England hotspot. *Earth and Planetary Science Letters*, *545*, 116352.

Mercuzot, M., Bourquin, S., Beccaletto, L., Ducassou, C., Rubi, R., & Pellenard, P. (2021). Palaeoenvironmental reconstitutions at the Carboniferous–Permian transition south of the Paris Basin, France: implications on the stratigraphic evolution and basin geometry. *International Journal of Earth Sciences*, *110*(1), 9–33.

Merle, O., & Michon, L. (2001). The formation of the West European Rift; a new model as exemplified by the Massif Central area. *Bulletin de La Societé Géologique de France*, *172*(2), 213–221.

Millot, R., Guerrot, C., Innocent, C., Négrel, P., & Sanjuan, B. (2011). Chemical, multi-isotopic (Li-B-Sr-U-H-O) and thermal characterization of Triassic formation waters from the Paris Basin. *Chemical Geology*, *283*(3–4), 226–241. https://doi.org/10.1016/j.chemgeo.2011.01.020

Millot, R., Négrel, P., & Petelet-Giraud, E. (2007). Multi-isotopic (Li, B, Sr, Nd) approach for geothermal reservoir characterization in the Limagne Basin (Massif Central, France). *Applied Geochemistry*, *22*(11), 2307–2325. https://doi.org/10.1016/j.apgeochem.2007.04.022

Moreira, M. (2013). Noble Gas Constraints on the Origin and Evolution of Earth's Volatiles. *Geochemical Perspectives*, *2*(2), 229–230.

Moreira, M., Rouchon, V., Muller, E., & Noirez, S. (2018). The xenon isotopic signature of the mantle beneath Massif Central. *Geochem. Perspect. Lett*, *6*, 28–32.

Morrison, P., & Pine, J. (1955). Radiogenic Origin of the Helium Isotopes in Rock. *Annals of the New York Academy of Sciences*, *62*(3), 71–92. https://doi.org/10.1111/j.1749-6632.1955.tb35366.x

Mukhopadhyay, S., & Parai, R. (2019). Noble gases: A record of earth's evolution and mantle dynamics. *Annual Review of Earth and Planetary Sciences*, *47*, 389–419. https://doi.org/10.1146/annurev-earth-053018-060238

Nehlig, P., Boivin, P., Goër, A., Mergoil, J., Prouteau, G., Sustrac, G., & Thiéblemont, D. (2003). Les volcans du Massif Central. *Geologues*, 130–131.

Oxburgh, E. R., O'Nions, R. K., & Hill, R. I. (1986). Helium isotopes in sedimentary basins. *Nature*, *324*(6098), 632–635. https://doi.org/10.1038/324632a0

Pasquet, G., Houssein Hassan, R., Sissmann, O., Varet, J., & Moretti, I. (2021). An Attempt to Study Natural H2 Resources across an Oceanic Ridge Penetrating a Continent: The Asal–Ghoubbet Rift (Republic of Djibouti). *Geosciences*, *12*(1), 16.

Petit, C., de Barros, L., Duclaux, G., & Mazabraud, Y. (2019). Why are there no earthquakes in the intracratonic paris basin? Insights from flexural models. *Geosciences (Switzerland)*, *9*(12). https://doi.org/10.3390/geosciences9120502

Pinti, D. L., & Marty, B. (1995). Noble gases in crude oils from the Paris Basin, France: Implications for the origin of fluids and constraints on oil-water-gas interactions. *Geochimica et Cosmochimica Acta*, *59*(16), 3389–3404. https://doi.org/10.1016/0016-7037(95)00213-J

Pinti, D. L., & Marty, B. (1998). The origin of helium in deep sedimentary aquifers and the problem of dating very old groundwaters. *Geological Society Special Publication*, *144*, 53–68. https://doi.org/10.1144/GSL.SP.1998.144.01.05

Prijac, C., Doin, M. P., Gaulier, J. M., & Guillocheau, F. (2000). Subsidence of the Paris Basin and its bearing on the late Variscan lithosphere evolution: A comparison between Plate and Chablis models. *Tectonophysics*, *323*(1–2), 1–38. https://doi.org/10.1016/S0040-1951(00)00100-1

Qin, S., Zhao, C., Li, Y., & Zhang, Y. (2015). Review of coal as a promising source of lithium. *International Journal of Oil, Gas and Coal Technology*, *9*(2), 215–229. https://doi.org/10.1504/IJOGCT.2015.067490

Raimbault, L., Cuney, M., Azencott, C., Duthou, J. L., & Joron, J. L. (1995). Geochemical evidence for a multistage magmatic genesis of Ta-Sn-Li mineralization in the granite at Beauvoir, French Massif Central. *Economic Geology*, *90*(3), 548–576. https://doi.org/10.2113/gsecongeo.90.3.548

Randazzo, P., Caracausi, A., Aiuppa, A., Cardellini, C., Chiodini, G., D'Alessandro, W., Li Vigni, L., Papic, P., Marinkovic, G., & Ionescu, A. (2021). Active Degassing of Deeply Sourced Fluids in Central Europe: New Evidences From a Geochemical Study in Serbia. *Geochemistry, Geophysics, Geosystems*, *22*(11), 1–17. https://doi.org/10.1029/2021GC010017

Regorda, A., Lardeaux, J.-M., Roda, M., Marotta, A. M., & Spalla, M. I. (2020). How many subductions in the Variscan orogeny? Insights from numerical models. *Geoscience Frontiers*, *11*(3), 1025–1052.

Risler, J. J. (1974). Description et classification géologique des sources minérales et thermales du Massif Central. *BRGM Report*, *74*.

Roger, J., Gaudry, F., Marteau, P., Quesnel, F., Chevremont, P., & Jauffret, D. (2010). Notice explicative, Carte géol. France (1/50 000), feuille Decize (549). *Orléans, BRGM*, *185*.

Sano, Y., & Marty, B. (1995). Origin of carbon in fumarolic gas from island arcs. *Chemical Geology*, *119*(1–4), 265–274.

Santos, F. J., López-Gutiérrez, J. M., García-León, M., Synal, H. A., & San Miguel, E. G. (2007). 129I record in a sediment core from Tinto River (Spain). *Nuclear Instruments and Methods in Physics Research, Section B: Beam Interactions with Materials and Atoms*, *259*(1), 503–507. https://doi.org/10.1016/j.nimb.2007.01.192

Seltzer, A. M., & Bekaert, D. v. (2022). A unified method for measuring noble gas isotope ratios in air, water, and volcanic gases via dynamic mass spectrometry. *International Journal of Mass Spectrometry*, *478*, 116873. https://doi.org/10.1016/j.ijms.2022.116873

Shuster, D. L., Farley, K. A., Sisterson, J. M., & Burnett, D. S. (2004). Quantifying the diffusion kinetics and spatial distributions of radiogenic 4He in minerals containing proton-induced 3He. *Earth and Planetary Science Letters*, *217*(1–2), 19–32. https://doi.org/10.1016/S0012-821X(03)00594-6

Sun, B., Zeng, F., Moore, T. A., Rodrigues, S., Liu, C., & Wang, G. (2022). Geochemistry of two high-lithium content coal seams, Shanxi Province, China. *International Journal of Coal Geology*, *260*, 104059.

Tolstikhin, I., Kamensky, I., Tarakanov, S., Kramers, J., Pekala, M., Skiba, V., Gannibal, M., & Novikov, D. (2010). Noble gas isotope sites and mobility in mafic rocks and olivine. *Geochimica et Cosmochimica Acta*, *74*(4), 1436–1447. https://doi.org/10.1016/j.gca.2009.11.001

Torgersen, T. (1993). Defining the role of magmatism in extensional tectonics: Helium 3 fluxes in extensional basins. *Journal of Geophysical Research*, *98*(B9), 16257. https://doi.org/10.1029/93JB00891

Vanderhaeghe, O., Laurent, O., Gardien, V., Moyen, J. F., Gébelin, A., Chelle-Michou, C., Couzinié, S., Villaros, A., & Bellanger, M. (2020). Flow of partially molten crust controlling construction, growth and collapse of the Variscan orogenic belt: The geologic record of the French Massif Central. *BSGF - Earth Sciences Bulletin*, *191*. https://doi.org/10.1051/bsgf/2020013

Wang, K., Brodholt, J., & Lu, X. (2015). Helium diffusion in olivine based on first principles calculations. *Geochimica et Cosmochimica Acta*, *156*, 145–153. https://doi.org/10.1016/j.gca.2015.01.023

Weinlich, F. H. (2005). Isotopically light carbon dioxide in nitrogen rich gases: The gas distribution pattern in the French Massif Central, the Eifel and the western Eger Rift. *Annals of Geophysics*, *48*(1), 19–31.

Fig 1
Geological map of the study area with helium isotope results (in R_a) and literature data. a) Structural map with major structures inherited from the Variscan orogeny (Baptiste, 2016). b) Simplified geological map (1/1,000,000 BRGM French geological map) with main geological structures of the area (Au: Aumance basin, De: Decize horst and Ma: Machine graben), location of the well SP4, SP7, springs and the lithium deposits of the area (Ch: Chanvence and Bv: Beauvoir; Gloaguen et al., 2018), and distribution of literature helium isotope data (Bräuer et al., 2017; Marty et al., 1993; Pinti & Marty, 1998). c) Focus on the Saint-Parize-le-Châtel area with location of the springs and wells. d) Simplified cross section line of the study area, with location on the map "b)" marked by the orange line.

Fig 2
$^4He/^{20}Ne$ versus $^3He/^4He$ plot. Samples plot in two groups, one with signatures close to a crustal source and the other with either a 2.5% input of mantle or with nucleogenic ^3He production consistent with the presence of 600 ppm Li. Lithium contents for the lower and upper limits of the European continental crust range are based on average values of U-Th for the continental crust (1.8 and 7.2 ppm, respectively; Krauskopf and Bird, 1967). $^4He/^{20}Ne$ values for SP4 are not precise due to ^{20}Ne abundances indistinguishable from baseline measurement. Massif Central and Paris Basin data are from the literature (Bräuer et al., 2017; Marty et al., 1993; Pinti & Marty, 1998).

Fig 3
Variation of helium isotope ratios with latitude. There is an apparent trend with decreasing $^3He/^4He$ ratios from south, starting at the Massif Central, to north, ending in the Paris Basin. Helium contents are higher for our dataset. Massif Central and Paris Basin data are from the literature (Bräuer et al., 2017; Marty et al., 1993; Pinti & Marty, 1998).

Fig 4
Three isotope diagram of neon. Mixing between air and solar, MORB (Sarda et al., 1988), Archean terrains (Lippmann-Pipke et al., 2011), crustal (Kennedy et al., 1990) end-members are displayed. SP4 plots between the crustal and Archean mixing lines with air and errors shown in 1 sigma level.

Fig 5
Xenon isotopic composition of SP7 gas corrected for physical fractionation. Data is expressed in δ (‰) of Xe ratios relative to atmospheric composition and normalised to ^{130}Xe. Error bars are 2 sigma. The SP7 gas has a clear ^{129}Xe excess that indicates mantle input.

Fig 6
$CO_2/^3He$ versus $\delta^{13}C$ plot (Sano and Marty, 1995). The dataset shows mixing between the three components and plots close to the MORB value while Massif Central data (Bräuer et al., 2017) only shows mixing between MORB and marine limestone. The grey field represents the MORB range from Marty & Zimmermann (1999).

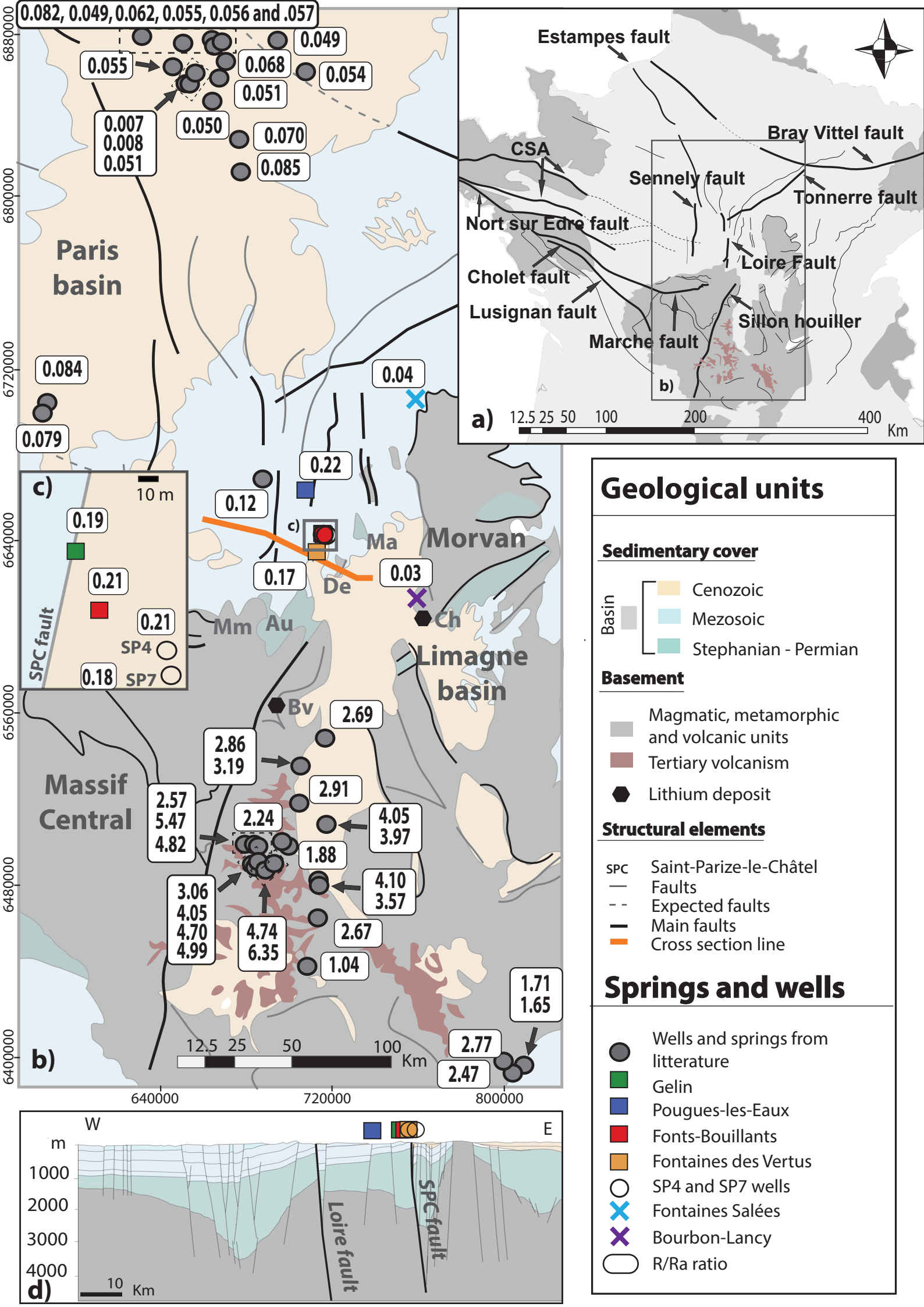
0.082, 0.049, 0.062, 0.055, 0.056 and .057
0.049
0.055
0.068
0.054
0.051
0.007
0.008
0.051
0.050
0.070
0.085
Paris basin
0.084
0.079
0.04
0.22
0.12
0.17
0.03
Ma
Morvan
De
Ch
Mm
Au
Limagne basin
Bv
2.69
2.86
3.19
2.91
Massif Central
2.57
5.47
4.82
2.24
4.05
3.97
1.88
4.10
3.57
3.06
4.05
4.70
4.99
4.74
6.35
2.67
1.04
1.71
1.65
2.77
2.47
12.5 25 50 100 Km
b)
640000
720000
800000
6880000
6800000
6720000
6640000
6560000
6480000
6400000
c)
10 m
0.19
0.21
0.21
SP4
0.18
SP7
SPC fault
a)
Estampes fault
Bray Vittel fault
CSA
Sennely fault
Tonnerre fault
Nort sur Edre fault
Loire Fault
Cholet fault
Lusignan fault
Sillon houiller
Marche fault
12.5 25 50 100 200 400 Km
W
E
m
1000
2000
3000
4000
Loire fault
SPC fault
10 Km
d)
Geological units
Sedimentary cover
Basin
Cenozoic
Mezosoic
Stephanian - Permian
Basement
Magmatic, metamorphic and volcanic units
Tertiary volcanism
Lithium deposit
Structural elements
SPC Saint-Parize-le-Châtel
Faults
Expected faults
Main faults
Cross section line
Springs and wells
Wells and springs from litterature
Gelin
Pougues-les-Eaux
Fonts-Bouillants
Fontaines des Vertus
SP4 and SP7 wells
Fontaines Salées
Bourbon-Lancy
R/Ra ratio

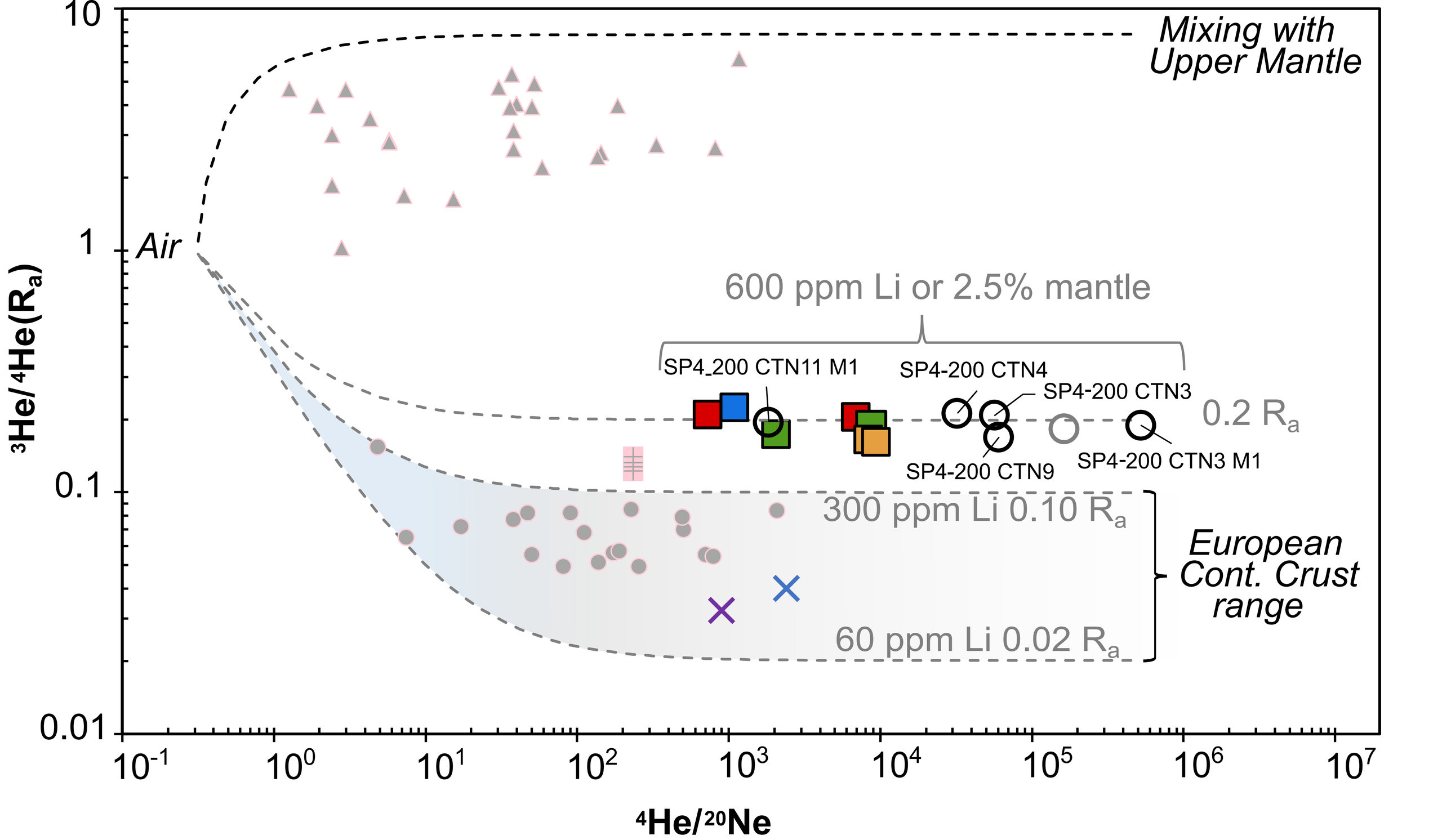
Mixing with Upper Mantle
Air
600 ppm Li or 2.5% mantle
SP4_200 CTN11 M1
SP4-200 CTN4
SP4-200 CTN3
0.2 Ra
SP4-200 CTN9
SP4-200 CTN3 M1
300 ppm Li 0.10 Ra
60 ppm Li 0.02 Ra
European Cont. Crust range
3He/4He(Ra)
4He/20Ne
10
1
0.1
0.01
10-1
100
101
102
103
104
105
106
107
Fonts-Bouillants
Gelin
Fontaine des Vertus
Pougues-les-Eaux
Fontaines Salées
Bourbon-Lancy
SP4
SP7
Massif Central
Paris basin basement
Paris basin

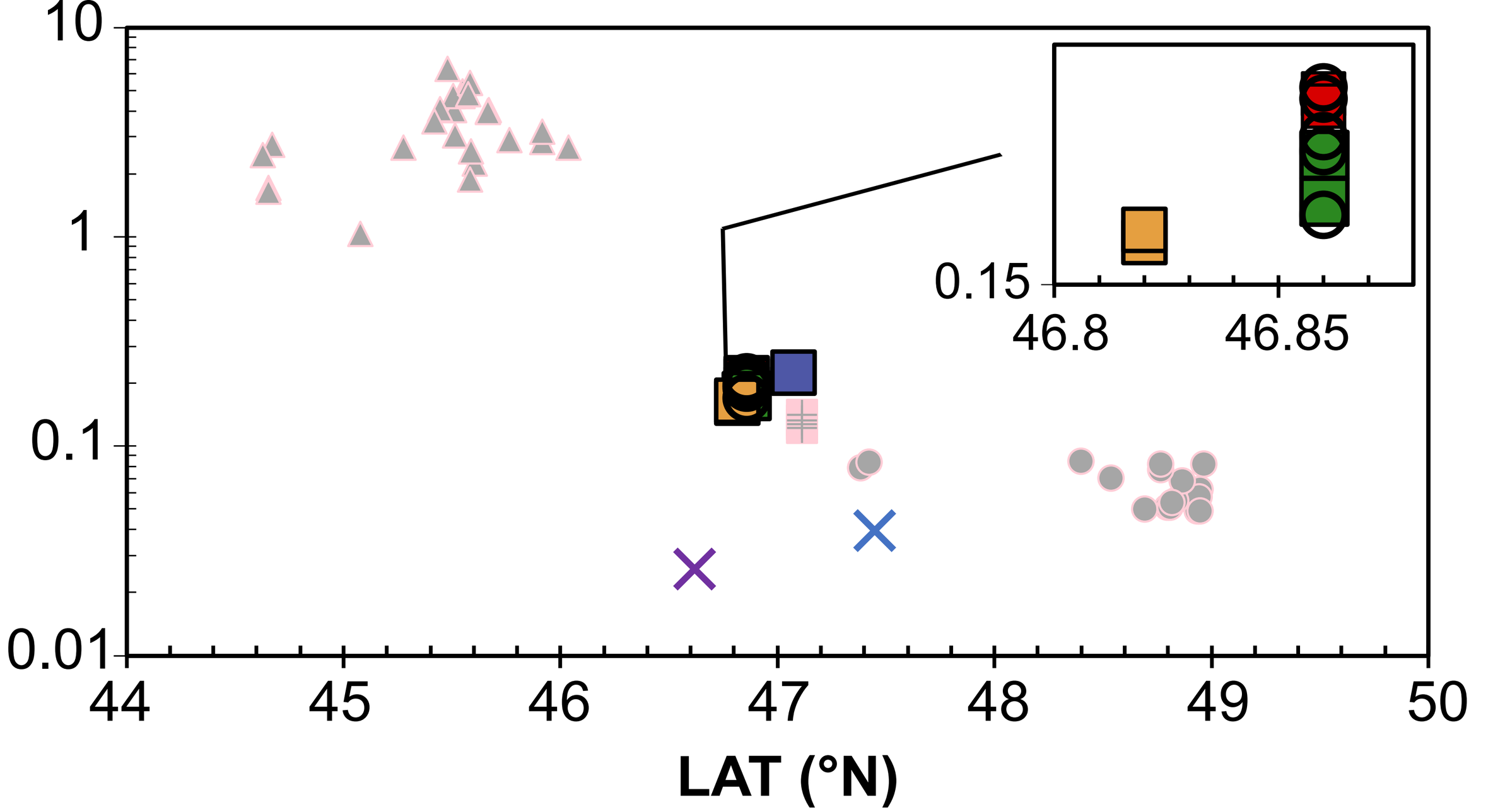
10
1
0.1
0.01
$^3He/^4He$ (R_a)
44
45
46
47
48
49
50
LAT (°N)
0.15
46.8
46.85
Fonts-Bouillants
Gelin
Fontaine des Vertus
SP4
Pougues-les-Eaux
Fontaines Salées
Bourbon-Lancy
Massif Central
Paris basin basement
Paris basin

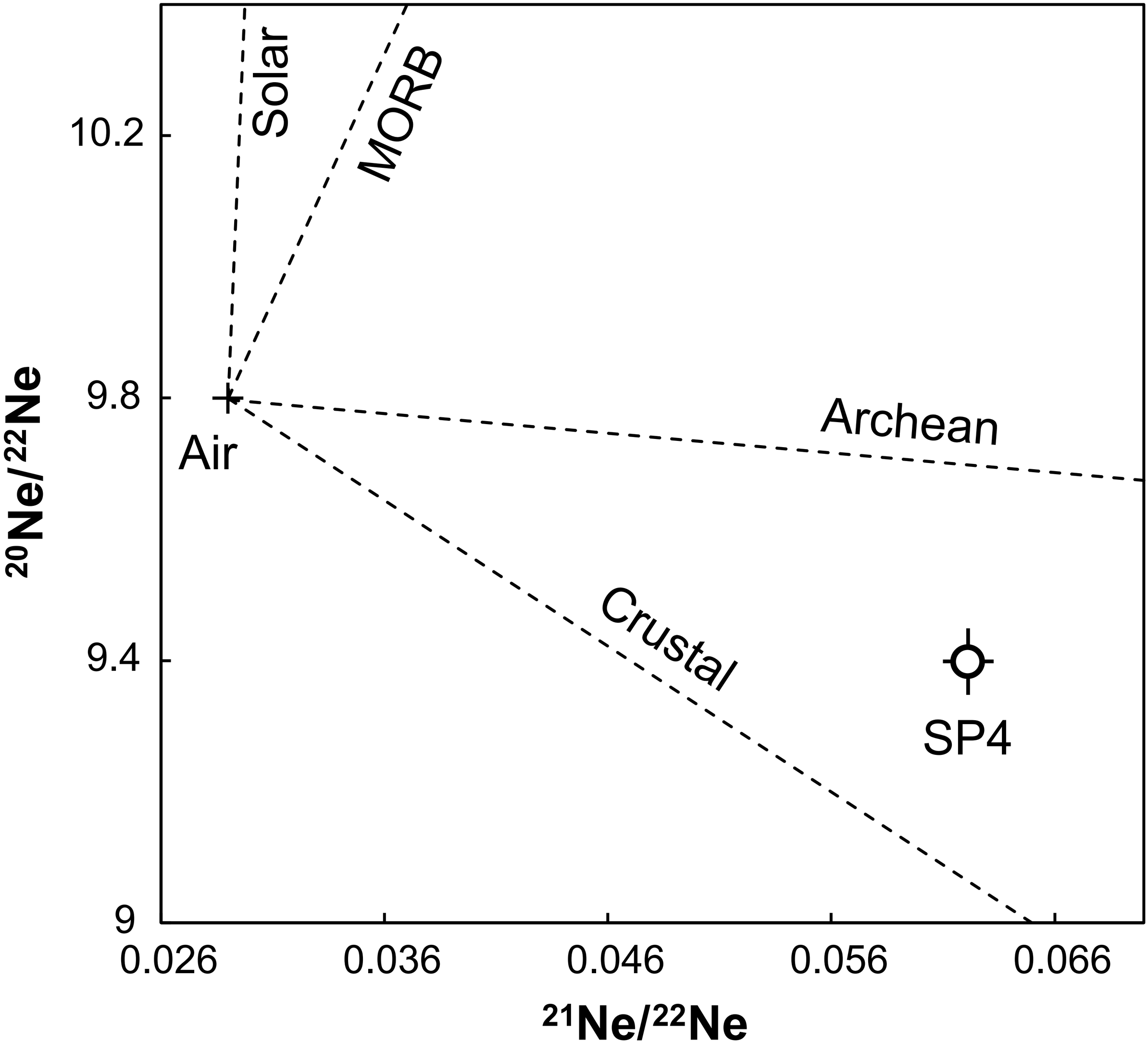
Solar
MORB
Air
Archean
Crustal
SP4
10.2
9.8
9.4
9
0.026
0.036
0.046
0.056
0.066
$^{20}Ne/^{22}Ne$
$^{21}Ne/^{22}Ne$

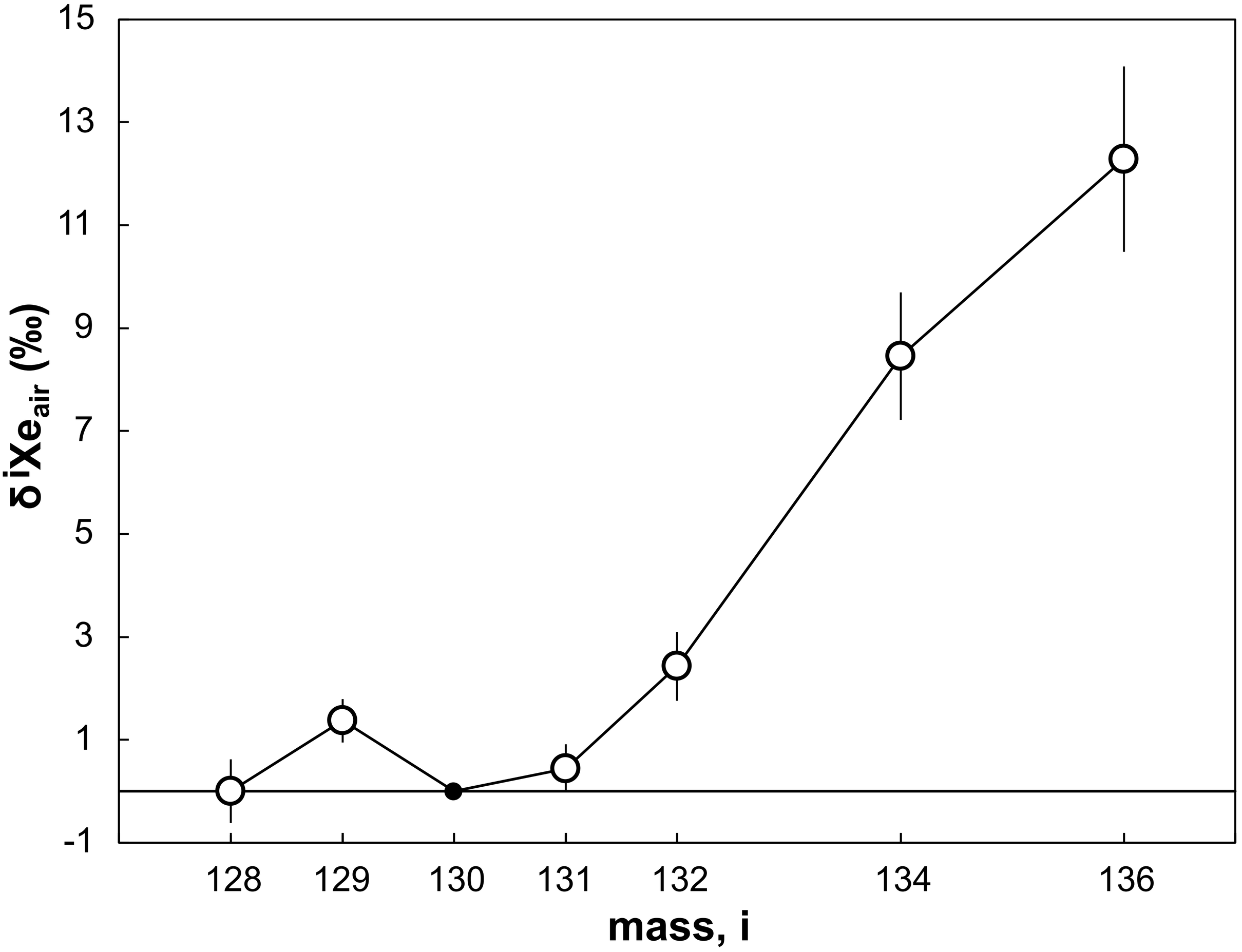
15
13
11
9
7
5
3
1
-1
δ iXe air (‰)
128
129
130
131
132
134
136
mass, i

Organic Sediment
←Sediment Fraction
Marine Limestone
←Mantle Fraction
Limestone Fraction→
$CO_2/^3He$
1.0E+13
1.0E+12
1.0E+11
1.0E+10
1.0E+09
6.0E+09
-11
-10
-9
MORB
-35
-30
-25
-20
-15
-10
-5
0
5
$\delta^{13}C$ (‰VPDB)
Fonts-Bouillants
Gelin
Pougues-les-Eaux
SP4
Massif Central

Table 1 List of sampled sites with coordinates, sampling dates, and average of main gas phase results from GC measurements. *A second sampling campaign occurred in May-June/2022 for $\delta^{15}N$ analyses.

Site	type	Date	map ref	LAT (°N)	LONG (°E)	CO_2 (vol.%)	N_2 (vol.%)	He (ppmV)
SP4	well	Aug-Sept/2022	1	46.85979	3.19336	93	5.6	394
SP7	well	Feb/2022	2	47.82861	4.18083	94	5.6	426
Gelin	spring	Aug-Sept/2022	3	46.86035	3.19268	91	6.1	416
Fonts-Bouillants	spring	Aug-Sept/2022	4	46.86008	3.19284	92	5.7	393
Fontaine des Vertus	spring	Aug-Sept/2022*	5	46.82025	3.17123	60	36.3	2874
Pougues-les-Eaux	spring	Aug-Sept/2022*	6	47.07635	3.09240	94	4	245
Fontaines Salées	spring	Aug-Sept/2022	7	47.44900	3.77680	0.9	92.5	45794
Bourbon-Lancy	spring	May-June/2022	8	46.61786	3.76974	2.6	91.3	20644

Table 2 $^{3}He/^{4}He$, $^{4}He/^{20}Ne$, $CO_2/^{3}He$, and stable isotopes results. $^{3}He/^{4}He$ are normalized by the atmospheric $^{3}He/^{4}He$ ratio (R_a – 1.39 x 10^{-6}; Graham, 2002). *Average $\delta^{15}N$ values from multiple measurements; SP4 value from two measurements performed on the same day (6.3 and 8.3 ‰) and Gelin from three measurements on different days (7.9, 8.5, and 8.9 ‰).

Site	Sample	$^{4}He/^{20}Ne$	$^{3}He/^{4}He$ (R_a)	$CO_2/^{3}He$	$\delta^{13}C$ (‰ vs PDB)	$\delta^{15}N$ (‰ vs Air)
SP4	SP4-100 CTN6	-	-	-	-10.1	7.3*
	SP4-200 CTN3	62080 ± 4724	0.21 ± 0.01	8.16E+09	-	-
	SP4-200 CTN3 M1	≤ 1656612	0.19 ± 0.01	8.96E+09	-	-
	SP4-200 CTN4	35291 ± 3003	0.21 ± 0.00	7.99E+09	-	-
	SP4-200 CTN9	66651 ± 5465	0.17 ± 0.01	1.00E+10	-	-
	SP4-200 CTN11 M1	1975 ± 55	0.20 ± 0.01	8.71E+09	-	-
SP7	SP7	180114 ± 34276	0.18 ± 0.01	8.66E+09	-	-
Gelin	GEL-100 CTN1	9509 ± 354	0.19 ± 0.00	8.37E+09	-10.0	8.4*
	GEL-300 CTN1 M1	2222 ± 72	0.17 ± 0.01	9.09E+09	-	-
Fonts-Bouillants	FBO-100 CTN1 M1	776 ± 22	0.21 ± 0.00	8.00E+09	-10.0	-
	FBO-300 CTN1 M1	7525 ± 281	0.21 ± 0.01	8.18E+09	-	-
Fontaine des Vertus	VER-100 CTN1	10240 ± 336	0.16 ± 0.01	9.26E+08	-	-
	VER-200 CTN1 M1	9042 ± 476	0.17 ± 0.00	9.06E+08	-11.8	7.5
Pougues-les-Eaux	POU-100 CTN1 M1	1170 ± 35	0.22 ± 0.01	1.22E+10	-10.3	6.1
Fontaines Salées	FON-100 CTN1 M1	2587 ± 66	0.04 ± 0.00	-	-20.0	7.1
Bourbon-Lancy	B-LANCY A	960 ± 20	0.03 ± 0.01	-	-	-

Table 3 Ne, Ar, and Xe isotope results. Xe ratios are reported in the delta notation relative to the atmospheric isotope composition. “corr” refers to data corrected for physical fractionation. Errors shown at 1 sigma.

Sample	$^{20}Ne/^{22}Ne$	$^{21}Ne/^{22}Ne$	$^{40}Ar/^{36}Ar$	$^{38}Ar/^{36}Ar$	δ vs Air, ‰					
					$^{128}Xe/^{130}Xe$	$^{129}Xe/^{130}Xe$	$^{131}Xe/^{130}Xe$	$^{132}Xe/^{130}Xe$	$^{134}Xe/^{130}Xe$	$^{136}Xe/^{130}Xe$
SP4-200-GB1	9.40 ± 0.05	0.0621 ± 0.0011	2866 ± 5	0.189 ± 0.001	-	-	-	-	-	-
SP4-100-GB1	-	-	2574 ± 11	0.179 ± 0.001	-	-	-	-	-	-
SP7 (raw)	-	-	696.6 ± 0.2	0.18840 ± 0.00002	0.996 ± 0.311	1.865 ± 0.145	-0.042 ± 0.179	1.463 ± 0.145	6.554 ± 0.167	9.464 ± 0.195
SP7 (corr)	-	-	-	-	0 ± 0.311	1.371 ± 0.212	0.445 ±0.235	2.430 ± 0.335	8.462 ± 0.619	12.286 ± 0.902